

# Power Kites for Wind Energy Generation

## Fast Predictive Control of Tethered Airfoils

BY MASSIMO CANALE, LORENZO FAGIANO, and MARIO MILANESE

**T**he problems posed by electric energy generation from fossil sources include high costs due to large demand and limited resources, pollution and CO<sub>2</sub> production, and the geopolitics of producer countries. These problems can be overcome by alternative sources that are renewable, cheap, easily available, and sustainable. However, current renewable technologies have limitations. Indeed, even the most optimistic forecast on the diffusion of wind, photovoltaic, and biomass sources estimates no more than a 20%

contribution to total energy production within the next 15–20 years.

Excluding hydropower plants, wind turbines are currently the largest source of renewable energy [1]. Unfortunately, wind turbines require heavy towers, foundations, and huge blades, which impact the environment in terms of land usage and noise generated by blade rotation, and require massive investments with long-term amortization. Consequently, electric energy production costs are not yet competitive with thermal generators, despite recent increases in oil and gas prices.

*Digital Object Identifier 10.1109/MCS.2007.909465*



**FIGURE 1** Kite surfing. Expert kite-surfers drive kites to obtain energy for propulsion. Control technology can be applied to exploit this technique for electric energy generation.



**FIGURE 2** KiteGen small-scale prototype of a yo-yo configuration. The kite lines are linked to two electric drives. The flight of the kite is controlled by regulating the pulling force on each line, and energy is generated as the kite unrolls the lines.

## THE KITEGEN PROJECT

To overcome the limitations of current wind power technology, the KiteGen project was initiated at Politecnico di Torino to design and build a new class of wind energy generators in collaboration with Sequoia Automation, Modelway, and Centro Studi Industriali. The project focus [2], [3] is to capture wind energy by means of controlled tethered airfoils, that is, kites; see Figure 1.

The KiteGen project has designed and simulated a small-scale prototype (see Figure 2). The two kite lines are rolled around two drums and linked to two electric drives, which are fixed to the ground. The flight of the kite is controlled by regulating the pulling force on each line. Energy is collected when the wind force on the kite unrolls the lines, and the electric drives act as generators due to the rotation of the drums. When the maximal line length of about 300 m is reached, the drives act as motors to recover the kite, spending a small percentage (about 12%, see the “Simulation Results” section for details) of the previously

generated energy [4]. This *yo-yo configuration* is under the control of the kite steering unit (KSU, see Figure 3), which includes the electric drives (for a total power of 40 kW), the drums, and all of the hardware needed to control a single kite. The aims of the prototype are to demonstrate the ability to control the flight of a single kite, to produce a significant amount of energy, and to verify the energy production levels predicted in simulation studies.

The potential of a similar yo-yo configuration is investigated, by means of simulation results, in [5] and [6] for one or more kites linked to a single cable. In [5] and [6], it is assumed that the angle of incidence of the kites can be controlled. Thus, the control inputs are not only the roll angle  $\psi$  and the cable winding speed, as considered in [4] and in this article, but also the lift coefficient  $C_L$ .

For medium-to-large-scale energy generators, an alternative KiteGen configuration is being studied, namely, the *carousel configuration*. In this configuration, introduced in [7] and shown in Figure 4, several airfoils are controlled by their KSUs placed on the arms of a vertical-axis rotor. The controller of each kite is designed to maximize the torque exerted on the rotor, which transmits its motion to an electric generator. For a given wind direction, each airfoil can produce energy for about 300° of carousel rotation; only a small fraction (about 1%, see the “Simulation Results” section for details) of the generated energy is used to drag the kite against the wind for the remaining 60°.

According to our simulation results, it is estimated that the required land usage for a kite generator may be lower than a current wind farm of the same power by a factor of up to 30–50, with electric energy

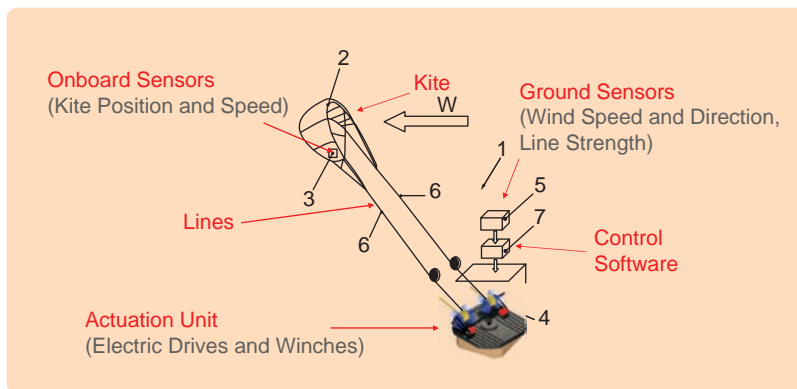


**FIGURE 3** Scheme of the kite steering unit. The kite steering unit, which provides automatic control for KiteGen, includes the electric drives, drums, and all of the hardware needed to control a single kite.

production costs lower by a factor up to 10–20. Such potential improvement over current wind technology is due to several aerodynamic and mechanical reasons [8], [9]. For example, 90% of the power generated by a 2-MW three-blade turbine with a 90-m rotor diameter is contributed by only the outer 40% of the blade area, corresponding to about 120 m<sup>2</sup>. This dependence is due to the fact that the aerodynamic forces on each infinitesimal section of the blades are proportional to the square of its speed with respect to the air, and this speed increases toward the tip of the blades. In KiteGen, the tethered airfoils act as the outer portions of the blades, without the need for mechanical support of the tower and of the less-productive inner blade portions; see Figure 5. Indeed, a mean generated power of 620 kW is obtained in the simulation reported in Figure 16 for a single kite of 100-m<sup>2</sup> area and 300-m line length.

Figure 5 shows that the torque exerted by wind forces at the base of a wind turbine's support structure increases with

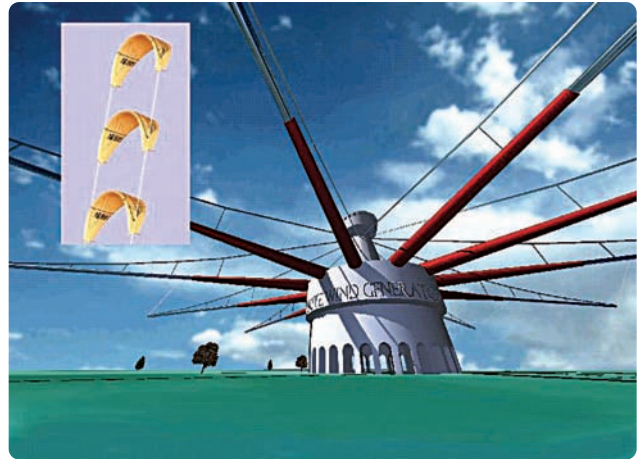


**FIGURE 4** KiteGen carousel configuration concept. Several airfoils are controlled by the kite steering units placed on the arms of a vertical axis rotor. The airfoils' flight is controlled so as to turn the rotor, which transmits its motion to an electric generator.

## KiteGen Project Perspectives

**A**t present, a small scale yo-yo prototype has been realized (see Figure S1). This system can generate up to 40 kW using commercial kites with characteristic area up to 10 m<sup>2</sup> and line length up to 800 m. The prototype is under test (see Figure S2). Preliminary tests show that the amount of energy predicted by simulation is confirmed by experimental data.

A new KiteGen prototype is expected to be built in the next 24–36 months to demonstrate the energy-generation capabilities of the carousel configuration. In particular, a carousel structure with a single kite steering unit mounted



**FIGURE S1** The first KiteGen prototype. Based on the yo-yo configuration, KiteGen can generate up to 40 kW using commercial kites with characteristic area up to 10 m<sup>2</sup> and line length up to 800 m. Preliminary tests show that the amount of energy predicted by simulation is confirmed by experimental data. A new KiteGen prototype is expected to be built in the next 24 to 36 months to demonstrate energy-generation capabilities of the carousel configuration.

on a cart riding on a circular rail will be considered. To collect the energy produced by the wagon motion, the wheels of the cart are connected to an alternator. Such a prototype is expected to produce about 0.5 MW with a rail radius of about 300 m. According to scalability, a platoon of carts, each one equipped with a kite steering unit, can be mounted on the rail to obtain a more effective wind power plant. This configuration can generate, on the basis of preliminary computations, about 100 MW at a production cost of about 20 €/MWh, which is two to three times lower than from fossil sources.



**FIGURE S2** KiteGen small scale prototype flying tests. This picture shows the kite motion and line developing during the traction phase. The kite steering unit is mounted on a light truck for easy transportation to locations with favorable wind conditions. This picture was taken on a hill near Torino.

the height of the tower, the force is independent of the line length in KiteGen. Due to structural and economical limits, it is not convenient to go beyond the 100–120 m height of the largest turbines commercially available. In contrast, airfoils can fly at altitudes up to several hundred meters, taking advantage of the fact that, as altitude over the ground increases, the wind is faster and less variable; see Figure 6. For example, at 800 m the mean wind speed doubles with respect to 100 m (the altitude at which the largest wind turbines operate). Since the power that can be extracted from wind grows with the cube of the wind speed, the possibility of reaching such heights represents a further significant advantage of KiteGen.

The carousel configuration is scalable up to several hundred megawatts, leading to increasing advantages over current wind farms. Using data from the Danish

Wind Industry Association Web site [10], it follows that, for a site such as Brindisi, in the south of Italy, a 2-MW wind turbine has a mean production of 4000 MWh/year. To attain a mean generation of 9 TWh/year, which corresponds to almost 1000-MW mean power, 2250 such towers are required, with a land usage of 300 km<sup>2</sup> and an energy production cost of about 100–120 €/MWh. In comparison, the production cost from fossil sources (gas, oil) is about 60–70 €/MWh. Simulation results show that a KiteGen capable of generating the same mean energy can be realized using 60–70 airfoils of about 500 m<sup>2</sup>, rotating in a carousel configuration of 1500-m radius and flying up to 800 m. The resulting land usage is 8 km<sup>2</sup>, and the energy production cost is estimated to be about 10–15 €/MWh.

## SYSTEM AND CONTROL TECHNOLOGIES NEEDED FOR KITEGEN

### Control Design

The main objective of KiteGen control is to maximize energy generation while preventing the airfoils from falling to the ground or the lines from tangling. The control problem can be expressed in terms of maximizing a cost function that predicts the net energy generation while satisfying constraints on the input and state variables. Nonlinear model predictive control (MPC) [11] is employed to accomplish these objectives, since it aims to optimize a given cost function and fulfill constraints at the same time. However, fast implementation is needed to allow real-time control at the required sampling time, which is on the order of 0.1 s. In particular, the implementation of fast model predictive control (FMPC) based on set membership approximation methodologies as in [12] and [13] is adopted, see “How Does FMPC Work?” for details.

### Model Identification

Optimizing performance for KiteGen relies on predicting the behavior of the system dynamics as accurately as possible. However, since accurately modeling the dynamics of a nonrigid airfoil is challenging, model-based control design may not perform satisfactorily on the real system. In this case, methods for identifying nonlinear systems [14], [15] can be applied to derive more accurate models.

### Sensors and Sensor Fusion

The KiteGen controller is based on feedback of the kite position and speed vector, which must be measured or accurately estimated. Each airfoil is thus equipped with a pair of triaxial accelerometers and a pair

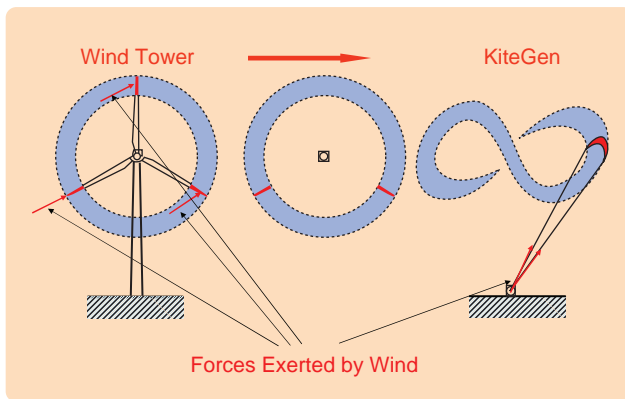


**FIGURE 5** Comparison between wind turbines and airfoils in energy production. In wind towers, limited blade portions (red) contribute predominantly to power production. In KiteGen, the kite acts as the most active portions of the blades, without the need for mechanical support of the less active portions and the tower.

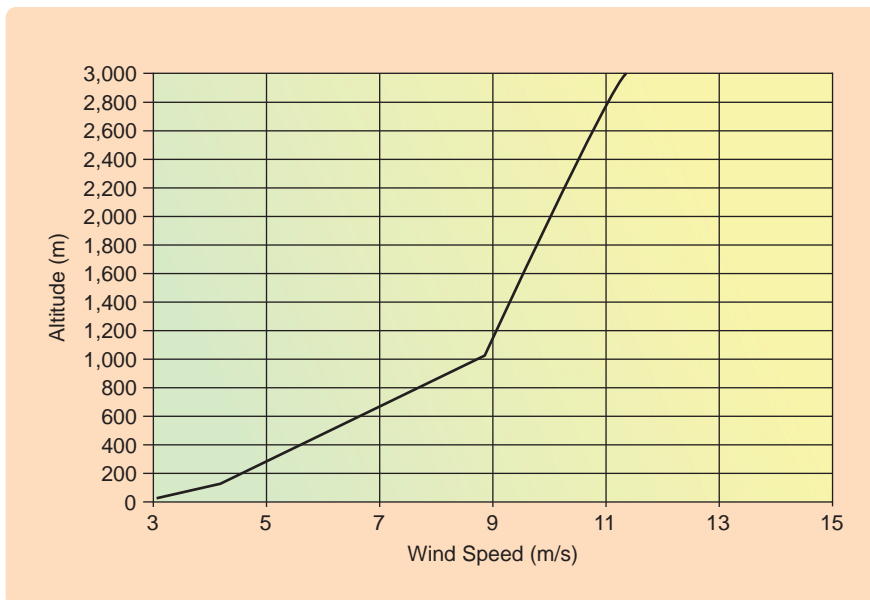


**FIGURE 6** Wind-speed variation as a function of altitude. These data are based on the average European wind speed of 3 m/s at ground level. Source: Delft University, Dr. Wubbo Ockels.

## How Does FMPC Work?

The fast model predictive control (FMPC) approach introduced and described in [12] and [13] is based on set membership techniques. The main idea is to find a function  $\hat{f}$  that approximates the exact predictive control law  $\psi(t_k) = f(w(t_k))$  to a specified accuracy. Evaluating the approximating function is faster than solving the constrained optimization problem considered in MPC design.

To be more specific, consider a bounded region  $W \subset \mathbb{R}^8$  where  $w$  can evolve. The region  $W$  can be sampled by choosing  $\tilde{w}_k \in W$ ,  $k = 1, \dots, \nu$ , and computing offline the corresponding exact MPC control given by

$$\tilde{\psi}_k = f(\tilde{w}_k), \quad k = 1, \dots, \nu. \quad (\text{S1})$$

The aim is to derive, from these known values of  $\tilde{\psi}_k$  and  $\tilde{w}_k$  and from known properties of  $f$ , an approximation  $\hat{f}$  of  $f$  over  $W$ , along with a measure of the approximation error. Neural networks are used in [S1] for such an approximation. However, neural networks have limitations, such as the possibility of local minima during the learning phase and the difficulty of satisfying the constraints in the image set of the function to be approximated. Moreover, no measure of the approximation error is provided. To overcome these drawbacks, a set membership approach is used in [12] for MPC with linear models. Based on sampled data and a priori information about  $f$ , the approach finds a feasible function set in which the true function is guaranteed to lie. An optimal approximation, along with approximation error, is derived based on this set. In the case of KiteGen control it is assumed that  $f \in \mathcal{F}_\gamma$ , where  $\mathcal{F}_\gamma$  is the set of Lipschitz functions on  $W$  with Lipschitz constant  $\gamma$ . Note that stronger assumptions cannot be made, since even in the simple case of linear dynamics and a quadratic functional,  $f$  is a piecewise linear continuous function [S2]. In addition, the input saturation condition gives the a priori bound  $|f(w)| \leq \bar{\psi}$ . This information about the function  $f$ , combined with the values of the function at the points  $\tilde{w}_k \in W$ ,  $k = 1, \dots, \nu$ , implies that  $f$  is a member of the feasible function set

$$FFS = \{f \in \mathcal{F}_\gamma : |f(w)| \leq \bar{\psi}; f(\tilde{w}_k) = \tilde{\psi}_k, \quad k = 1, \dots, \nu\}, \quad (\text{S2})$$

which summarizes the available information on  $f$ . Set membership theory facilitates the derivation of an optimal estimate of  $f$  and its approximation error in terms of the  $L_p(W)$  norm for  $p \in [1, \infty]$ , where  $\|f\|_p \doteq [\int_W |f(w)|^p dw]^{1/p}$ ,  $p \in [1, \infty)$ , and  $\|f\|_\infty \doteq \text{ess-sup}_W |f(w)|$ . For given  $\hat{f} \approx f$ , the related  $L_p$  approximation error is  $\|f - \hat{f}\|_p$ . Since the true function  $f$  is known at only a finite number of points, the error between  $\hat{f}$  and  $f$  is unknown. However, given the a priori information, the tightest guaranteed bound is given by

$$\|f - \hat{f}\|_p \leq \sup_{\tilde{f} \in FFS} \|\tilde{f} - \hat{f}\|_p \doteq E(\hat{f}), \quad (\text{S3})$$

where  $E(\hat{f})$  is the (guaranteed) approximation error.

A function  $f^*$  is optimal approximation if

$$r_p \doteq E(f^*) = \inf_{\tilde{f}} E(\tilde{f}),$$

where the radius of information  $r_p$  gives the minimal  $L_p$  approximation error that can be guaranteed. Defining

$$\bar{f}(w) \doteq \min \left[ \bar{\psi}, \min_{k=1, \dots, \nu} (\tilde{\psi}_k + \gamma \|w - \tilde{w}_k\|) \right], \quad (\text{S4})$$

$$\underline{f}(w) \doteq \max \left[ -\bar{\psi}, \max_{k=1, \dots, \nu} (\tilde{\psi}_k - \gamma \|w - \tilde{w}_k\|) \right], \quad (\text{S5})$$

yields the function

$$f^*(w) = \frac{1}{2} [\bar{f}(w) + \underline{f}(w)], \quad (\text{S6})$$

which is an optimal approximation in the  $L_p(W)$  norm for all  $p \in [1, \infty]$  [13]. Moreover, the approximation error of  $f^*$  is pointwise bounded as

$$|f(w) - f^*(w)| \leq \frac{1}{2} |\bar{f}(w) - \underline{f}(w)|, \quad \text{for all } w \in W$$

and is pointwise convergent to zero [13]

$$\lim_{\nu \rightarrow \infty} |f(w) - f^*(w)| = 0, \quad \text{for all } w \in W, \quad (\text{S7})$$

Thus, evaluating  $\sup_{w \in W} |\bar{f}(w) - \underline{f}(w)|$ , it is possible to decide whether the values of  $\tilde{w}_1, \dots, \tilde{w}_\nu$ , chosen for the offline computation of  $\tilde{\psi}_k$  are sufficient to achieve a desired accuracy in the estimation of  $f$  or if the value of  $\nu$  must be increased. Then, the MPC control can be approximately implemented online by evaluating the function  $f^*(w_k)$  at each sampling time so that

$$\psi_{t_k} = f^*(w_k).$$

As  $\nu$  increases, the approximation error decreases at the cost of increased computation time.

## REFERENCES

- [S1] T. Parisini and R. Zoppoli, "A receding-horizon regulator for nonlinear systems and a neural approximation," *Automatica*, vol. 31, no. 10, pp. 1443–1451, 1995.
- [S2] A. Bemporad, M. Morari, V. Dua, and E.N. Pistikopoulos "The explicit linear quadratic regulator for constrained systems," *Automatica*, vol. 38, pp. 3–20, 2002

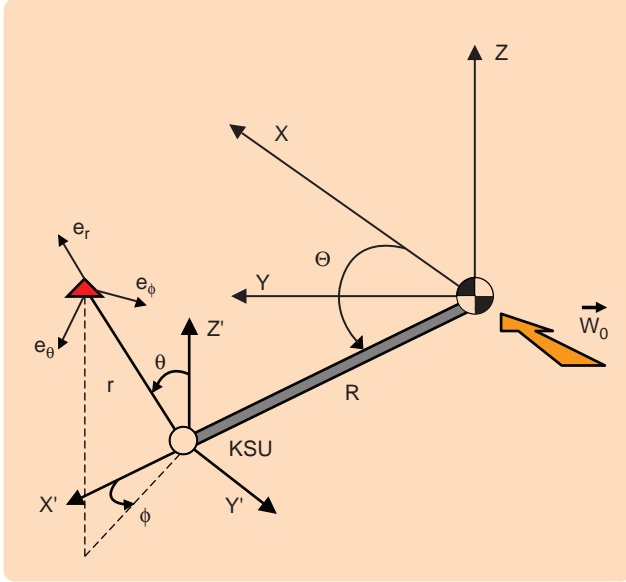


**FIGURE 7** Model of a single kite steering unit. A fixed cartesian coordinate system  $(X, Y, Z)$  is considered, with the  $X$  axis aligned with the direction of the nominal wind speed vector  $\vec{W}_0$ . A second cartesian coordinate system  $(X', Y', Z')$ , centered at the KSU location, is considered when KSU is moving with respect to  $(X, Y, Z)$ . In the yo-yo configuration, since the KSU location is fixed at the ground,  $(X', Y', Z') \equiv (X, Y, Z)$  is assumed. In the carousel configuration, the KSU rotates around the origin of  $(X, Y, Z)$  at distance  $R$ , with angular speed  $\dot{\theta}$ . The local coordinate system  $(\vec{e}_\theta, \vec{e}_\phi, \vec{e}_r)$  is also shown.

of triaxial magnetometers placed at the airfoil's extreme edges, which transmit data to the control unit by means of radio signals. These data are sufficient for estimating the kite position and speed. However, in order to improve estimation accuracy and to achieve some degree of recovery in the case of sensor failure, we plan to use a load cell to measure the length and traction force of each line as well as a vision system to determine the kite angular position.

A key issue in KiteGen operation is the detection and recovery of possible breakdowns or malfunctions of the sensors. For example, the vision system may not operate in the presence of clouds, haze, or heavy rain. A common way to treat this problem is to use estimation techniques based on the system model and available measurements. However, due to the kite's nonlinear dynamics, the extended Kalman filter (EKF), based on approximations of the nonlinearities, gives rise to numerical stability problems and severe accuracy deterioration. Moreover, the EKF design is based on a model that, although quite complex and nonlinear, is only an approximate description of the actual system. Alternatively, the direct virtual sensor (DVS) approach [16], [17] facilitates the design of an optimal filter based on experimental data collected in the absence of sensor faults. In particular, when an accurate model is available and the noise statistical hypotheses are

fulfilled, the DVS gives the same accuracy as the theoretical minimal variance filter. Moreover, in the presence of modeling errors and nonlinearities, the DVS guarantees stability and performs tradeoffs between optimality and robustness, which are not achievable with EKF.

## KITE GENERATOR MODELS

### Kite Dynamics

The model developed in [18] describes the kite dynamics. A fixed cartesian coordinate system  $(X, Y, Z)$  is considered (see Figure 7), with the  $X$  axis aligned with the nominal wind speed vector. The wind speed vector is represented as  $\vec{W}_I = \vec{W}_0 + \vec{W}_t$ , where  $\vec{W}_0$  is the nominal wind, assumed to be known and expressed in  $(X, Y, Z)$  as

$$\vec{W}_0 = \begin{pmatrix} W_x(Z) \\ 0 \\ 0 \end{pmatrix}, \quad (1)$$

where  $W_x(Z)$  is a known function that gives the wind nominal speed at each altitude  $Z$  (see Figure 6). The term  $\vec{W}_t$  may have components in all directions and is assumed to be unknown, accounting for unmeasured turbulence.

A second cartesian coordinate system  $(X', Y', Z')$ , centered at the KSU location, is introduced to take into account possible KSU motion with respect to  $(X, Y, Z)$ ; otherwise,  $(X', Y', Z') \equiv (X, Y, Z)$  is assumed. In this system, the kite position can be expressed as a function of its distance  $r$  from the origin and the angles  $\theta$  and  $\phi$ , as depicted in Figure 7, which also shows the basis vectors  $e_\theta, e_\phi, e_r$  of a local coordinate system centered at the kite location.

Applying Newton's laws of motion to the kite in the local coordinate system yields

$$\ddot{\theta} = \frac{F_\theta}{m r}, \quad (2)$$

$$\ddot{\phi} = \frac{F_\phi}{m r \sin \theta}, \quad (3)$$

$$\ddot{r} = \frac{F_r}{m}, \quad (4)$$

where  $m$  is the kite mass, and the forces  $F_\theta, F_\phi$ , and  $F_r$  include the contributions of the gravitational force  $mg$ , apparent force  $\vec{F}_{app}$ , aerodynamic force  $\vec{F}_{aer}$ , and the force  $F_c$  exerted by the lines on the kite. Expressed in the local coordinates, the forces are given by

$$F_\theta = (\sin \theta)mg + F_{app,\theta} + F_{aer,\theta}, \quad (5)$$

$$F_\phi = F_{app,\phi} + F_{aer,\phi}, \quad (6)$$

$$F_r = -(\cos \theta)mg + F_{app,r} + F_{aer,r} - F_c. \quad (7)$$

### Apparent Forces

The components of the apparent force vector  $\vec{F}_{app}$  depend on the kite generator configuration. For example, for the yo-yo

configuration, centrifugal inertial forces have to be considered, that is,  $\vec{F}_{\text{app}} = \vec{F}_{\text{app}}(\theta, \phi, r, \dot{\theta}, \dot{\phi}, \dot{r})$ . For the carousel configuration, since each KSU moves along a circular trajectory with constant radius  $R$  (see Figure 7), the carousel rotation angle  $\Theta$  and its derivatives must be included in the apparent force calculation, so that  $\vec{F}^{\text{app}} = \vec{F}^{\text{app}}(\theta, \phi, r, \Theta, \dot{\theta}, \dot{\phi}, \dot{r}, \dot{\Theta}, \ddot{\Theta})$ .

### Aerodynamic Forces

The aerodynamic force  $\vec{F}_{\text{aer}}$  depends on the effective wind speed  $\vec{W}_e$ , which in the local system is computed as

$$\vec{W}_e = \vec{W}_a - \vec{W}_l, \quad (8)$$

where  $\vec{W}_a$  is the kite speed with respect to the ground. For both the yo-yo and carousel configurations,  $\vec{W}_a$  can be expressed as a function of the local coordinate system  $(\phi, \theta, r)$  and the position of the KSU with respect to the fixed coordinate system  $(X, Y, Z)$ .

Let us consider now the kite wind coordinate system, with its origin located at the kite center of gravity, the basis vector  $\vec{x}_w$  aligned with the effective wind speed vector, the basis vector  $\vec{z}_w$  contained by the kite longitudinal plane of symmetry and pointing from the top surface of the kite to the bottom, and the basis vector  $\vec{y}_w$  completing a right-handed system. In the wind coordinate system the aerodynamic force  $\vec{F}_{\text{aer},w}$  is given by

$$\vec{F}_{\text{aer},w} = F_D \vec{x}_w + F_L \vec{z}_w, \quad (9)$$

where  $F_D$  is the drag force and  $F_L$  is the lift force, computed as

$$F_D = -\frac{1}{2} C_D A \rho |W_e|^2, \quad (10)$$

$$F_L = -\frac{1}{2} C_L A \rho |W_e|^2, \quad (11)$$

where  $\rho$  is the air density,  $A$  is the kite characteristic area, and  $C_L$  and  $C_D$  are the kite lift and drag coefficients. All of these variables are assumed to be constant. The aerodynamic force  $\vec{F}_{\text{aer}}$  can then be expressed in the local coordinate system as a nonlinear function of several arguments of the form

$$\vec{F}_{\text{aer}} = \begin{pmatrix} F_{\text{aer},\theta}(\theta, \phi, r, \psi, \vec{W}_e) \\ F_{\text{aer},\phi}(\theta, \phi, r, \psi, \vec{W}_e) \\ F_{\text{aer},r}(\theta, \phi, r, \psi, \vec{W}_e) \end{pmatrix}. \quad (12)$$

The kite roll angle  $\psi$  in (12) is the control variable, defined by

$$\psi = \arcsin\left(\frac{\Delta l}{d}\right), \quad (13)$$

where  $d$  is the kite width and  $\Delta l$  is the length difference between the two lines (see Figure 8). The roll angle  $\psi$  influences the kite motion by changing the direction of  $\vec{F}_{\text{aer}}$ .

### Line Forces

Concerning the effect of the lines, the force  $F_c$  is always directed along the local unit vector  $e_r$  and cannot be negative, since the kite can only pull the lines. Moreover,  $F_c$  is measured by a force transducer on the KSU, and, through control of the electric drives, it is regulated so that the line speed satisfies  $\dot{r}(t) \approx \dot{r}_{\text{ref}}(t)$ , where  $\dot{r}_{\text{ref}}(t)$  is chosen. In the case of the yo-yo configuration,  $F_c(t) = F_c(\theta, \phi, r, \dot{\theta}, \dot{\phi}, \dot{r}, \dot{r}_{\text{ref}}, \vec{W}_e)$ , while, for the carousel configuration,  $F_c(t) = F_c(\theta, \phi, r, \Theta, \dot{\theta}, \dot{\phi}, \dot{r}, \dot{\Theta}, \dot{r}_{\text{ref}}, \vec{W}_e)$ .

### Motor Dynamics

In the case of the carousel configuration, the motion law for the generator rotor is taken into account by the equation

$$J_z \ddot{\Theta} = R F_c(\sin \theta) \sin \phi - T_c, \quad (14)$$

where  $J_z$  is the rotor moment of inertia and  $T_c$  is the torque of the electric generator/motor linked to the rotor. Viscous terms are neglected in (14) since the rotor speed  $\dot{\Theta}$  is kept low as shown in the ‘‘Simulation Results’’ section.  $T_c$  is positive when the kite is pulling the rotor with increasing values of  $\Theta$ , thus generating energy, and it is negative when the electric generator is acting as a motor to drag the rotor when the kite is not able to generate a pulling force. The torque  $T_c$  is set by a local controller to keep the rotor at constant speed  $\dot{\Theta} = \dot{\Theta}_{\text{ref}}$ .

### KiteGen Dynamics Description

The generic system dynamics are of the form

$$\dot{x}(t) = g(x(t), u(t), W_x(t), \dot{r}_{\text{ref}}(t), \dot{\Theta}_{\text{ref}}(t), \vec{W}_l(t)), \quad (15)$$

where  $x(t) = [\theta(t) \phi(t) r(t) \Theta(t) \dot{\theta}(t) \dot{\phi}(t) \dot{r}(t) \dot{\Theta}(t)]^T$  are the model states and  $u(t) = \psi(t)$  is the control variable. In the case of the yo-yo configuration,  $\Theta = \dot{\Theta} = \dot{\Theta}_{\text{ref}} = 0$ . All of the model states are assumed to be measured or estimated for use in feedback control. Mechanical power  $P$  generated

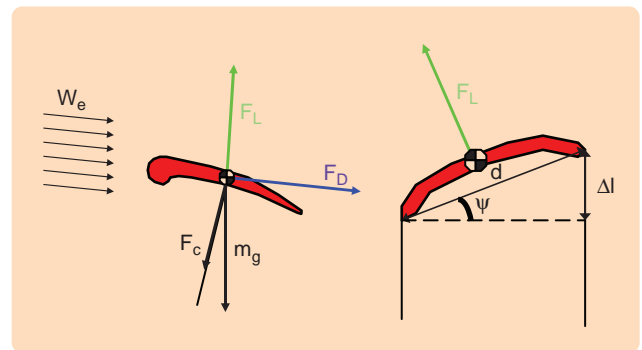


**FIGURE 8** Forces acting on the kite. The aerodynamic lift and drag forces are  $F_L$  and  $F_D$ , respectively, the gravitational force is  $m_g$ , and the pulling force  $F_c$  is exerted by the lines. The length difference between the lines gives the roll input angle  $\psi$ .

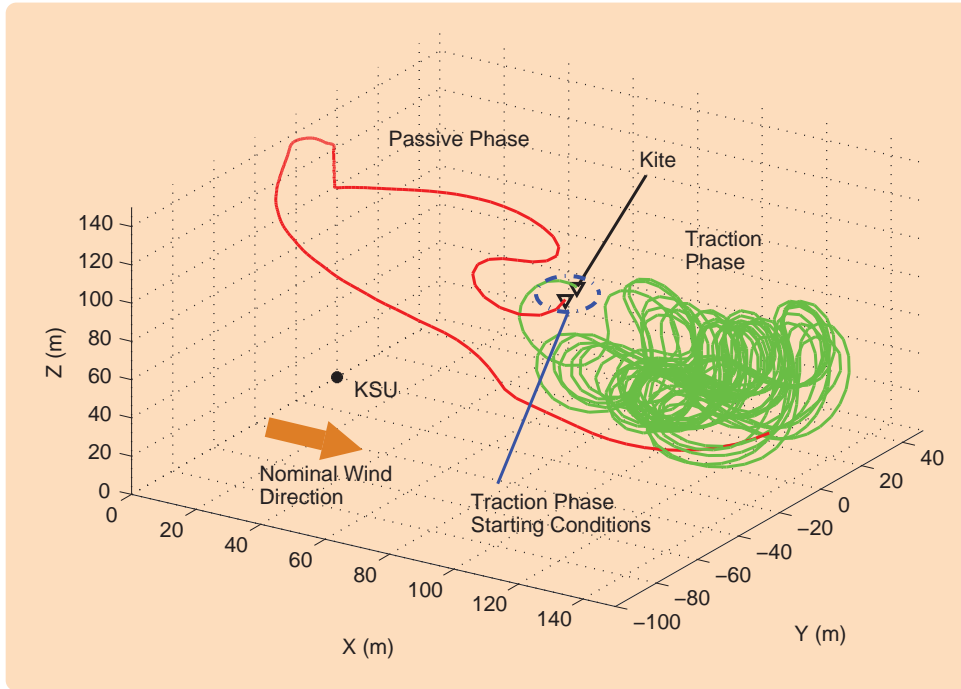


**FIGURE 9** Yo-yo configuration phases. The kite steering unit acts on the kite lines in such a way that energy is generated in the traction phase (green) and spent in the passive phase (red). Each cycle begins when the proper starting conditions (circled in blue) are satisfied. In this simulation the effects of turbulence are neglected.

with KiteGen is the sum of the power generated by unrolling the lines and the power generated by the rotor movement, that is,

$$P(t) = \dot{r}(t)F_c(t) + \dot{\Theta}(t)T_c(t). \quad (16)$$

Both terms in (16) can be negative when the kite lines are being recovered in the yo-yo configuration or the rotor is being dragged against the wind in the carousel configuration. For the yo-yo configuration the term  $\dot{\Theta}T_c$  is zero, and thus the generated mechanical energy is due only to line unrolling. Note that (16) is related to a carousel with a single KSU. When more kites are linked to the same carousel, the effect of line rolling/unrolling for each kite must be included.

### KITEGEN CONTROL

To investigate the potential of KiteGen and to assist in the design of physical prototypes, a controller is designed for use in numerical simulations. In particular, the mathematical models of the yo-yo and carousel configurations described in the section “Kite Generator Models” are used to design nonlinear model predictive controllers.

In both KiteGen configurations, energy is generated by continually performing a two-phase cycle. In the first phase, the kite exploits wind power to generate mechanical energy until a condition is reached that impairs further energy generation. In the second phase, the kite is recovered to a suitable position to start another productive phase. These phases are referred to as the *traction phase* and

*passive phase*, respectively. Thus, different MPC controllers are designed to control the kite in the traction and passive phases. For the overall cycle to be productive, the total amount of energy produced in the first phase must be greater than the energy spent in the second phase. Consequently, the controller employed in the traction phase must maximize the produced energy, while the objective of the passive phase controller is to maneuver the kite to the traction-phase initial position with minimal energy. The main reason for using MPC is that input and state constraints must be imposed, for example, to keep the kite sufficiently far from the

ground and to account for actuator physical limitations. Moreover, other constraints on the state variables are added to force the kite to follow figure-eight trajectories to prevent the lines from tangling.

### MPC for KiteGen

MPC is a model-based control technique that handles both state and input constraints. With MPC, the computation of the control variable is performed at discrete time instants defined on the basis of a suitably chosen sampling period  $\Delta t$ . Without wind disturbances, (15) becomes

$$\dot{x}(t) = g(x(t), u(t), W_x(t), \dot{r}_{\text{ref}}(t), \dot{\Theta}_{\text{ref}}(t)),$$

where  $u(t) = \psi(t)$  is the control variable. At each sampling time  $t_k = k\Delta t$ , the measured values of the state  $x(t_k)$  and the wind speed  $W_x(t_k)$ , together with the reference speeds  $\dot{r}_{\text{ref}}(t_k)$ ,  $\dot{\Theta}_{\text{ref}}(t_k)$  are used to compute the control  $u(t)$  through the performance index

$$J(U, t_k, T_p) = \int_{t_k}^{t_k+T_p} L(\tilde{x}(\tau), \tilde{u}(\tau), W_x(\tau), \dot{r}_{\text{ref}}(\tau), \dot{\Theta}_{\text{ref}}(\tau))d\tau, \quad (17)$$

where  $T_p = N_p\Delta t$ , is the prediction horizon of  $N_p$  steps,  $\tilde{x}(\tau)$  is the state predicted inside the prediction horizon according to (15) using  $\vec{W}_t(t) = 0$  and  $\tilde{x}(t_k) = x(t_k)$ , and the piecewise constant control input  $\tilde{u}(t)$  belonging to the sequence  $U = \{\tilde{u}(t)\}$ ,  $t \in [t_k, t_k+T_p]$  is defined as

$$\tilde{u}(t) = \begin{cases} \bar{u}_i, & \text{for all } t \in [t_i, t_{i+1}], i = k, \dots, k + T_c - 1, \\ \bar{u}_{k+T_c-1}, & \text{for all } t \in [t_i, t_{i+1}], i = k + T_c, \dots, k + T_p - 1, \end{cases} \quad (18)$$

where  $T_c = N_c \Delta t$ , and  $N_c \leq N_p$  is the control horizon. The function  $L(\cdot)$  in (17) is defined to maximize the energy generated in the traction phase and minimize the energy spent in the passive phase. Moreover, to account for physical limitations on both the kite behavior and the control input  $\psi$ , constraints of the form  $\tilde{x}(t) \in \mathbb{X}$ ,  $\tilde{u}(t) \in \mathbb{U}$  can be included. In particular, to keep the kite sufficiently far from the ground, the state constraint

$$\theta(t) \leq \bar{\theta}$$

is considered with  $\bar{\theta} < \pi/2$ . Actuator physical limitations are taken into account by the constraints

$$\begin{aligned} |\psi(t)| &\leq \bar{\psi}, \\ |\dot{\psi}(t)| &\leq \bar{\dot{\psi}}. \end{aligned}$$

Tables 2 and 4 provide details on the values of  $\bar{\psi}$  and  $\bar{\dot{\psi}}$  for the yo-yo and carousel configurations, respectively. Additional constraints are added to force the kite to follow figure-eight trajectories rather than circular ones to prevent the tangling of the lines. Such constraints force the angle  $\phi$  to oscillate at half the frequency of the angle  $\theta$ , thus generating the desired kite trajectory.

The predictive control law, which is computed using a receding horizon strategy, is a nonlinear static function of the system state  $x$ , the nominal measured wind speed  $W_x$ , and the reference speeds  $\dot{r}_{\text{ref}}$ ,  $\dot{\theta}_{\text{ref}}$  of the form

$$\psi(t_k) = f(x(t_k), W_x(t_k), \dot{r}_{\text{ref}}(t_k), \dot{\theta}_{\text{ref}}(t_k)). \quad (19)$$

### Yo-Yo Configuration Controller

The traction phase begins when the kite is flying in a prescribed zone downwind of the KSU, at a suitable altitude  $Z_I$  with a given line length  $r_0$  (see Figure 9).

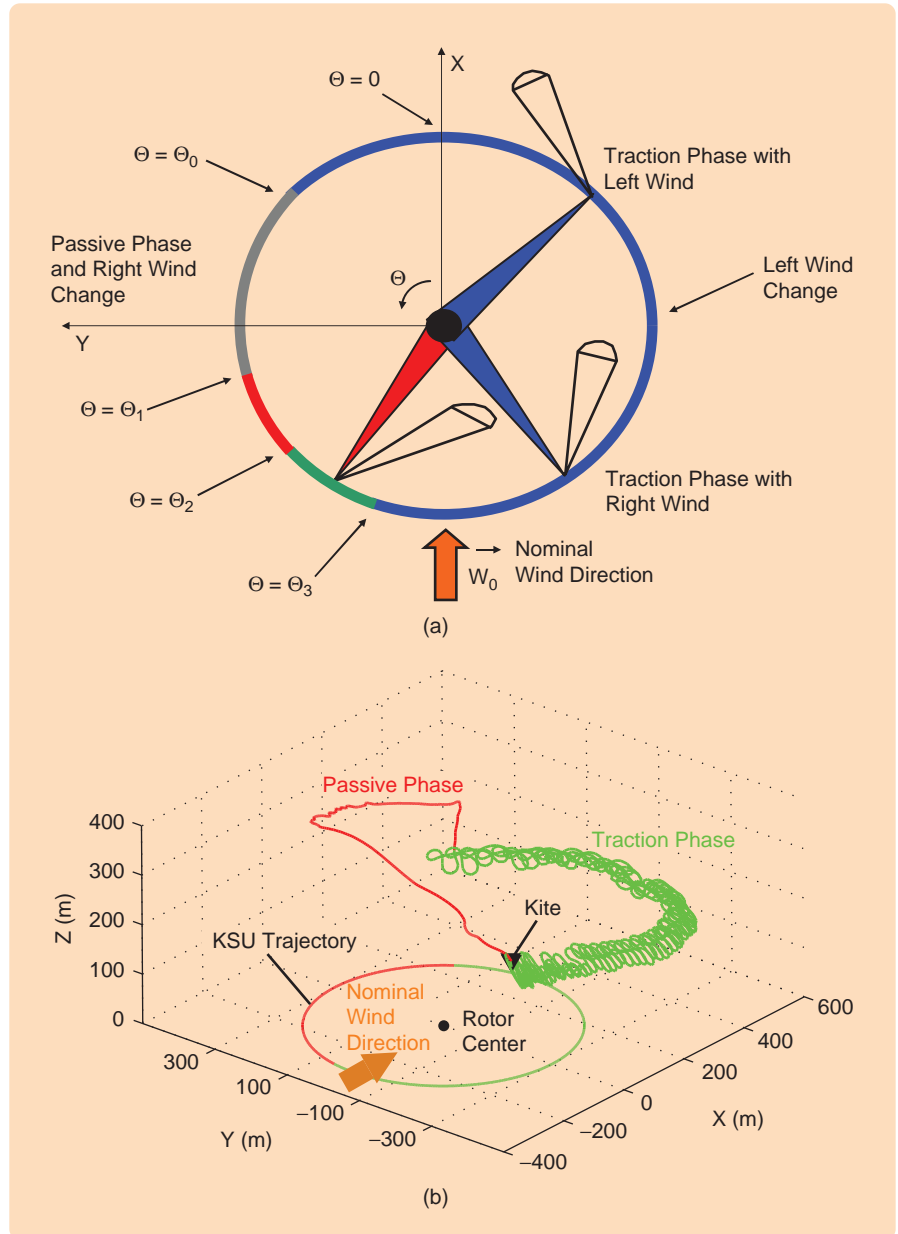


**FIGURE 10** (a) Carousel configuration phases. The same rotor arm is depicted with three subsequent angular values. The passive phase starts when the rotor arm reaches the angular position  $\theta_0$ , and lasts until the rotation angle  $\theta_3$  is reached. To maneuver the kite to a suitable position to begin the traction phase (highlighted in blue), the passive phase is divided into 3 subphases (gray, orange, and green) delimited by rotation angles  $\theta_1$  and  $\theta_2$ . (b) Kite trajectory with carousel configuration. The kite follows figure-eight orbits, which maximize its speed during the traction phase (green), while during the passive phase (red) the airfoil speed is very low to reduce drag forces. The kite steering unit follows a circular trajectory at ground height, with radius  $R$ .

When the traction phase starts, the kite flies as line length  $r$  increases due to a positive value  $\dot{r}_{\text{ref}}$  of the line

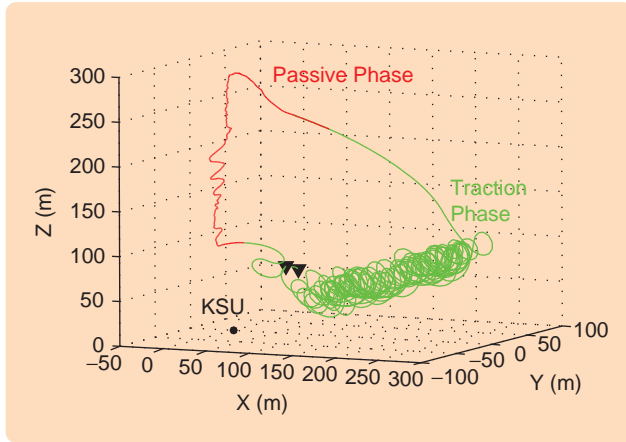


**FIGURE 11** Simulation results for the yo-yo configuration. Kite trajectories are reported during the traction (green) and passive (red) phases of a complete yo-yo configuration cycle in the presence of wind turbulence. Note that the behavior is similar to Figure 9 despite the turbulence.

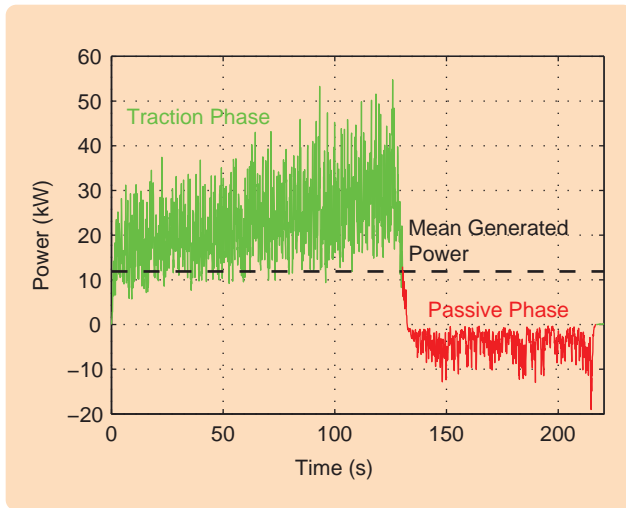


**FIGURE 12** Simulated power obtained with the yo-yo configuration. A complete cycle is considered in the presence of wind turbulence. The instantaneous course of the generated power during the traction phase (green) is reported together with the power spent for the kite recovery in the passive phase (red). The mean value of the power generated during the cycle, which is represented by a dashed line, is 11.8 kW. The corresponding generated energy is 2613 kJ per cycle.

speed reference provided by the local motor controller. Since a traction force  $F_c$  is created on the kite lines, the system generates mechanical power. The predictive control law computes the line angle  $\psi$  (see Figure 8) in order to vary  $F_c$  and thus optimize the aerodynamic behavior of the kite for energy generation. The line angle  $\psi$  is obtained by varying  $\Delta l$  according to (13) by imposing a setpoint on the desired line length achieved by the local motor controller.

The value of the reference line speed  $\dot{r}_{\text{ref}}$  is chosen as a compromise between obtaining high traction force action

and high line winding speed. Basically, the stronger the wind, the higher the value of  $\dot{r}_{\text{ref}}$  that can be set while obtaining high force values. The control system objective in the traction phase is to maximize the energy generated during the prediction interval  $[t_k, t_k + T_p]$ . Since the instantaneous generated mechanical power is  $P(t) = \dot{r}(t)F_c(t)$ , MPC minimizes the cost function

$$J(t_k) = - \int_{t_k}^{t_k+T_p} \dot{r}(\tau)F_c(\tau)d\tau. \quad (20)$$

The traction phase ends when the length of the lines reaches a given value  $\bar{r}$  and the passive phase begins.

The passive phase is divided into three subphases. In the first subphase, the line speed  $\dot{r}(t)$  is controlled to smoothly decrease toward zero. The control objective is to move the kite into a zone with low values of  $\theta$  and high values of  $|\phi|$  (see Figure 7), where the effective wind speed  $\bar{W}_e$  and force  $F_c$  are low and the kite can be recovered with low energy expense. Then, in the second subphase,  $\dot{r}(t)$  is controlled to smoothly decrease from zero to a negative value, which provides a compromise between high rewinding speed and low force  $F_c$ . During this passive subphase, the control objective is to minimize the energy spent to rewind the lines. This second subphase ends when the line length  $r$  reaches the desired minimum value. In the third passive subphase,  $\dot{r}(t)$  is controlled to smoothly increase toward zero from the previous negative setpoint. The control objective is to move the kite in the traction phase starting zone. The passive phase ends when the starting conditions for the traction phase are reached.

### Carousel Configuration Controller

In the carousel configuration (see figures 4 and 10), the torque  $T_c$  given by the carousel motor/generator is such

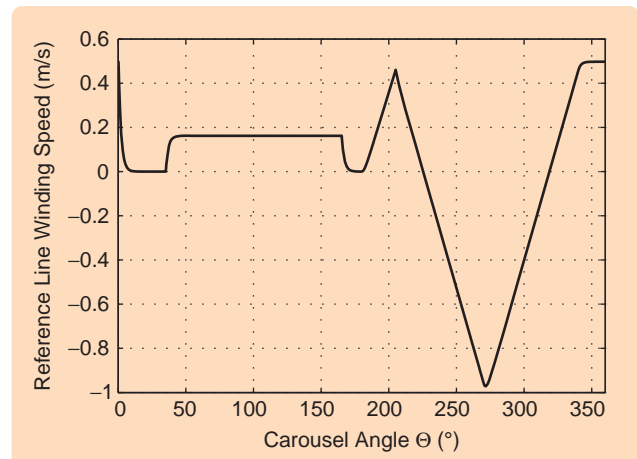


**FIGURE 13** Line speed reference imposed during a complete carousel cycle. The commanded line speed  $\dot{r}(t)$  is chosen on the basis of simulation data to increase the mean generated power and to ensure that the lengths of the lines at the beginning of each cycle are the same.

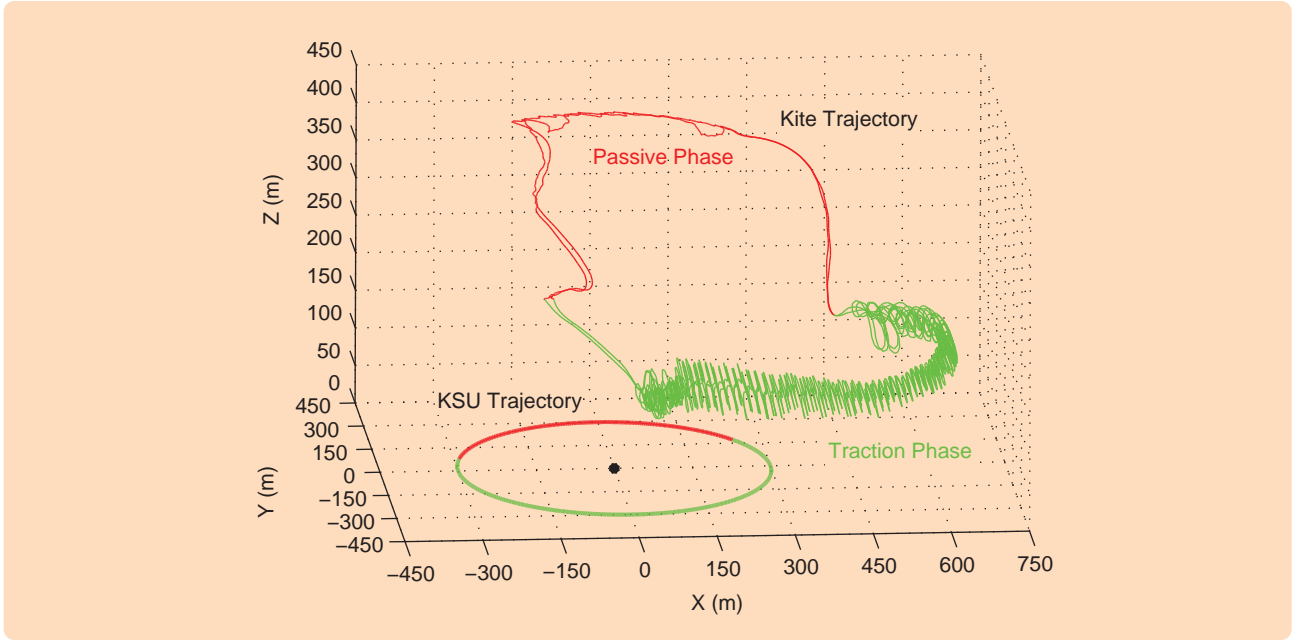


**FIGURE 14** Simulation results for the carousel configuration. Kite and kite steering unit trajectories are reported during traction (green) and passive (red) phases related to two complete cycles in the presence of turbulence. Note that, despite the turbulence, the trajectories show good repeatability.

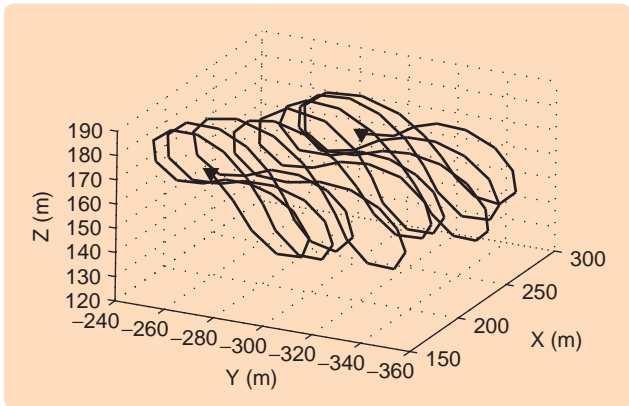


**FIGURE 15** Figure-eight kite orbits during the traction phase for the carousel configuration. Such orbits are imposed by means of suitable constraints on the angles  $\theta$  and  $\phi$  to avoid line wrapping.

that the rotor moves at the constant reference angular speed  $\dot{\Theta}_{ref}$ , which is chosen to optimize the net energy generated in the cycle. Since the angular speed is constant, each kite can be controlled independently, provided that the lines never collide. Thus, a single kite is considered in the following. The traction phase begins at the rotor angular position  $\Theta = \Theta_3$ , where the nominal wind direction is such that the kite can pull the rotor arm [see Figure 10(a)]. A suitable trajectory for the line speed  $\dot{r}$  during the traction phase is set to further increase generated power. Recalling that mechanical power obtained at each instant is the sum of the effects given by line unrolling and rotor movement, MPC minimizes the cost function

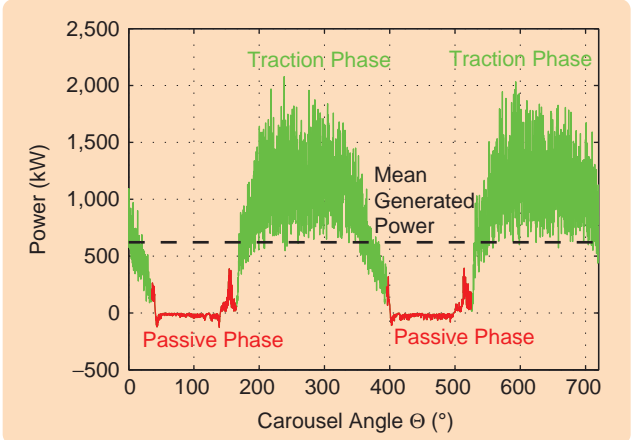


**FIGURE 16** Power generated with the carousel configuration. Two complete cycles are considered in the presence of wind turbulence. The instantaneous course of the generated power during the traction phases (green) is reported together with the power required for the kite recovery in the passive phases (red). Note the nearly null values of energy usage during the passive phases. The mean value of the power generated during the two cycles is 621 kW and is represented by a dashed line. The corresponding generated energy is 234 MJ per cycle.

$$J(t_k) = - \int_{t_k}^{t_k+T_p} \dot{r}(\tau)F_c(\tau) + \dot{\Theta}(\tau)T_{gen}(\tau)d\tau. \quad (21)$$

When the rotor arm reaches the angle  $\Theta_0$ , the kite can no longer pull the carousel, and the traction phase ends. Then, the passive phase starts, and the electric generator linked to the rotor acts as a motor to drag the carousel between angles  $\Theta_0$  and  $\Theta_3$ . Meanwhile, the kite is moved to a suitable position for initiating the next traction phase.

**TABLE 1** Model and control parameters of the simulated yo-yo configuration. Note, in particular, the small characteristic area and low aerodynamic efficiency.

Symbol	Numeric Value	Description and Units
$m$	2.5	Kite mass (kg)
$A$	5	Characteristic area (m <sup>2</sup> )
$\rho$	1.2	Air density (kg/m <sup>3</sup> )
$C_L$	1.2	Lift coefficient
$C_D$	0.15	Drag coefficient
$E = \frac{C_L}{C_D}$	8	Aerodynamic efficiency
$\bar{r}$	1.5	Traction phase reference for $\dot{r}$ (m/s)
$\underline{r}$	-2.5	Passive phase reference for $\dot{r}$ (m/s)
$T_c$	0.1	Sample time (s)
$N_c$	1	Control horizon
$N_p$	25	Prediction horizon

**TABLE 2** State and input constraints and cycle starting and ending conditions for the simulated yo-yo configuration. The traction phase starts when  $\theta \geq \theta_I$ ,  $|\phi - \phi_I| \leq 5^\circ$ , and  $r < r_I$ . The passive phase starts when  $r > \bar{r}$ . State and input constraints are imposed throughout the cycle.

Constraint Definition	Constraint Description
$\underline{\theta}_I = 40^\circ$	Traction phase starting conditions
$\phi_I = 0^\circ$	
$r_I = 105$ m	
$\bar{r} = 290$ m	Maximum line length
$ \theta(t)  \leq 85^\circ$	State constraint
$ \psi(t)  \leq 4^\circ$	Input constraints
$ \dot{\psi}(t)  \leq 20^\circ/\text{s}$	

**TABLE 3** Model and control parameters for the carousel configuration. Despite the low aerodynamic efficiency, this structure can generate a significant amount of energy as shown by the results reported in Figure 16.

Symbol	Numeric Value	Description and Units
$m$	50	Kite mass (kg)
$A$	100	Characteristic area (m <sup>2</sup> )
$J_z$	$910^8$	Rotor moment of inertia (kg-m <sup>2</sup> )
$R$	300	Rotor radius (m)
$\rho$	1.2	Air density (kg/m <sup>3</sup> )
$C_L$	1.2	Lift coefficient
$C_D$	0.15	Drag coefficient
$E = \frac{C_L}{C_D}$	8	Aerodynamic efficiency
$\dot{\Theta}_{\text{ref}}$	0.16	Reference $\dot{\Theta}$ (rev/min)
$T_c$	0.2	Sample time (s)
$N_c$	1	Control horizon (steps)
$N_p$	5	Prediction horizon (steps)

The passive phase is divided into three subphases. Transitions between subphases are marked by suitable values  $\Theta_1$  and  $\Theta_2$  of the rotor angle [see Figure 10(a)], which are chosen to minimize the total energy spent dur-

**TABLE 4** Objectives and starting conditions for the cycle phases and state and input constraints for the carousel configuration. In the passive phase, the controller is designed to drive  $\theta$  to  $\theta_I$  during the first subphase,  $\phi$  to  $\phi_I$  during the second subphase, and  $\theta$  to  $\theta_{II}$  during the third subphase. These values are chosen to minimize the energy used to return the kite to its position at the beginning of the traction phase. In particular, small values of  $\theta$  and  $\phi$  correspond to zones with low values of the effective wind speed and the tangential component of the pulling force  $F_c$  [see (14)]. State and input constraints are imposed throughout the cycle.

Constraint Definition	Constraint Description
$\Theta_0 = 35^\circ$	Passive phase starting condition
$\theta_I = 20^\circ$	First passive subphase objective
$\Theta_1 = 135^\circ$	Second passive subphase starting condition
$\phi_I = 140^\circ$	Third passive subphase objective
$\Theta_2 = 150^\circ$	Third passive subphase starting condition
$\theta_{II} = 50^\circ$	Third passive subphase objective
$\Theta_3 = 165^\circ$	Traction phase starting condition
$ \theta(t)  \leq 85^\circ$	State constraint
$ \psi(t)  \leq 3^\circ$	Input constraints
$ \dot{\psi}(t)  \leq 20^\circ/\text{s}$	

ing the passive phase. In the first subphase, the control objective is to move each kite to a zone with a low value of  $\theta$  [see figures 7 and 10(b)], where the effective wind speed  $\bar{W}_e$  and pulling force component tangential to the carousel  $F_c \sin \theta \sin \phi$  are much lower. At  $\Theta = \Theta_1$ , the second passive subphase begins, where the objective is to change the kite angular position  $\phi$  toward  $\phi_I$  to begin the traction phase. At  $\Theta = \Theta_2$ , the third passive subphase begins, where the control objective is to increase the kite angle  $\theta$  toward  $\theta_{II}$  to prepare the generator for the subsequent traction phase. For details, see [7].

## SIMULATION RESULTS

Simulations of the KiteGen system were performed using the wind speed model

$$W_x(Z) = \begin{cases} 0.04Z + 8 \text{ m/s}, & \text{if } Z \leq 100 \text{ m}, \\ 0.0171(Z - 100) + 12 \text{ m/s}, & \text{if } Z > 100 \text{ m}. \end{cases} \quad (22)$$

The nominal wind speed is 8 m/s at 0 m altitude, while the wind speed grows linearly to 12 m/s at 100 m altitude and up to 17.2 m/s at 300 m altitude. Moreover, wind turbulence  $\bar{W}_t$  is introduced, with uniformly distributed random components along the inertial axes ( $X$ ,  $Y$ ,  $Z$ ). The absolute value of each component of  $\bar{W}_t$  ranges from 0 m/s to 3 m/s, which corresponds to 36% of the nominal wind speed at 100 m altitude.

### Yo-Yo Configuration

For simulation, we consider a yo-yo configuration similar to the physical prototype. The numerical values of the kite

model and control parameters are reported in Table 1, while Table 2 contains the state values for the start and end conditions of each phase as well as the values of the state and input constraints.

Figure 11 shows the trajectory of the kite, while the power generated during the cycle is reported in Figure 12. The mean power is 11.8 kW, which corresponds to energy generation of 2613 kJ per cycle.

### Carousel Configuration

A carousel with a single KSU is considered. The model and control parameters employed are reported in Table 3, while Table 4 contains the start and end conditions for each phase, as well as the values of the state and input constraints. The line speed during the cycle is reported in Figure 13. This reference trajectory is chosen on the basis of the previous simulation to maximize the mean generated power and to ensure that the length of the lines at the beginning of each cycle is the same.

Figure 14 shows the trajectories of the kite and the control unit during two full cycles in the presence of random wind disturbances. Figure 15 depicts some orbits traced by the kite during the traction phase, while the power generated during the two cycles is reported in Figure 16. The mean power is 621 kW, and the generated energy is 234 MJ per cycle. Figure 17 depicts the course of the effective wind speed  $|\bar{W}_e|$  (see the section “Kite Generator Models” for details). It can be noted that during the traction phase the mean effective wind speed is about 14 times greater than the tangential speed of the rotor connected to the generator, which is 18 km/h. Since the fixed coordinate system  $(X, Y, Z)$  is defined on the basis of the nominal wind direction, a measurable change of the latter can be overcome by rotating the whole coordinate system  $(X, Y, Z)$ , thus obtaining the same performance without changing either the control system parameters or the starting conditions of the various phases.

### ACKNOWLEDGMENTS

KiteGen project is partially supported by Regione Piemonte under the Project “Controllo di aquiloni di potenza per la generazione eolica di energia” and by Ministero dell’Università e della Ricerca of Italy under the National Project “Advanced control and identification techniques for innovative applications.”

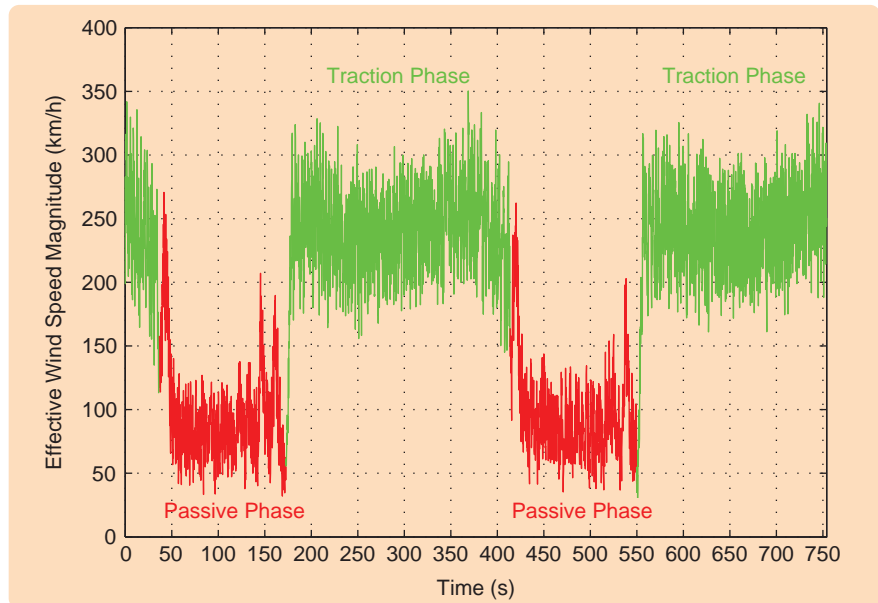


**FIGURE 17** Simulated effective wind speed for the carousel configuration. The course of  $|\bar{W}_e|$  during the traction subphases (green) and the passive subphases (red) is related to two complete carousel cycles. The average values are 250 km/h during the traction phase and 85 km/h during the passive phase.

### REFERENCES

- [1] “Renewables 2005: Global status report” Renewable Energy Policy Network, Worldwatch Institute, Wash. D.C., 2005 [Online]. Available: <http://www.REN21.net>
- [2] M. Ippolito, “Smart control system exploiting the characteristics of generic kites or airfoils to convert energy,” European patent 02840646, Dec. 2004.
- [3] M. Milanese and M. Ippolito “Automatic control system and process for the flight of kites,” International Patent PCT/IT2007/00325, May 2007.
- [4] M. Canale, L. Fagiano, M. Ippolito, and M. Milanese, “Control of tethered airfoils for a new class of wind energy generator,” in *Proc. 45th IEEE Conf. Decision and Control*, San Diego, CA, pp. 2006, 4020–4026.
- [5] B. Houska and M. Diehl, “Optimal control for power generating kites,” in *Proc. 9th European Control Conf.*, Kos, Greece, 2007, pp. 3560–3567.
- [6] A.R. Podgaets and W.J. Ockels, “Flight control of the high altitude wind power system,” in *Proc. 7th Conf. Sustainable Applications Tropical Island States*, Cape Canaveral, FL, 2007, pp. 125–130.
- [7] M. Canale, L. Fagiano, M. Milanese, and M. Ippolito, “KiteGen project: Control as key technology for a quantum leap in wind energy generators,” in *Proc. 26th American Control Conf.*, New York, 2007, pp. 3522–3528.
- [8] A. Betz, *Introduction to the Theory of Flow Machines*. New York: Pergamon, 1966.
- [9] M.L. Loyd, “Crosswind kite power,” *J. Energy*, vol. 4, no. 3, pp. 106–111, 1980.
- [10] Danish Association of Wind Industry Web site [Online]. Available: [www.windpower.org](http://www.windpower.org)
- [11] D.Q. Mayne, J.B. Rawlings, C.V. Rao, and P.O.M. Scokaert, “Constrained model predictive control: Stability and optimality,” *Automatica*, vol. 36, pp. 789–814, 2000.
- [12] M. Canale and M. Milanese, “FMPC: A fast implementation of model predictive control,” in *Proc. 16th IFAC World Congress*, Prague, Czech Republic, July 2005.
- [13] M. Canale, L. Fagiano, and M. Milanese, “Fast implementation of predictive controllers using SM methodologies,” in *Proc. 46th IEEE Conf. Decision and Control*, New Orleans, LA, 2007.
- [14] M. Milanese and C. Novara, “Set membership identification of nonlinear systems,” *Automatica*, vol. 40, pp. 957–975, 2004.
- [15] M. Milanese and C. Novara, “Structured set membership identification of nonlinear systems with application to vehicles with controlled suspensions,” *Control Eng. Practice*, vol. 15, pp. 1–16, 2007.
- [16] K. Hsu, M. Milanese, C. Novara, and K. Poolla, “Nonlinear virtual

sensors design from data," in *Proc. IFAC Symp. System Identification (SYSID)*, Newcastle, Australia, pp. 576–581, 2006.

[17] K. Hsu, M. Milanese, C. Novara, and K. Poolla, "Filter design from data: Direct vs. two-step approaches," in *Proc. 25th American Control Conf.*, Minneapolis, MN, 2006, pp. 1606–1611.

[18] M. Diehl, "Real-time optimization for large scale nonlinear processes," Ph.D. dissertation, University of Heidelberg, Germany, 2001 [Online]. Available: [http://www.iwr.uni-heidelberg.de/~Moritz.Diehl/DISSERTATION/diehl\\_diss.pdf](http://www.iwr.uni-heidelberg.de/~Moritz.Diehl/DISSERTATION/diehl_diss.pdf)

## AUTHOR INFORMATION

**Massimo Canale** received the Laurea degree in electronic engineering (1992) and the Ph.D. in systems engineering (1997), both from the Politecnico di Torino, Italy. From 1997 to 1998, he worked as a software engineer in the R&D department of Comau Robotics, Italy. Since 1998, he has been an assistant professor in the Dipartimento di Automatica e Informatica of the Politecnico di Torino. His research interests include robust control, model predictive control, set membership approximation, and application to automotive and aerospace problems.

**Lorenzo Fagiano** received the master's degree in automotive engineering in 2004 from Politecnico di Torino, Italy. In 2005 he worked at Centro Ricerche Fiat, Italy, in the active vehicle systems area. Since January 2006 he has been a Ph.D. student at Politecnico di Torino. His main research interests include constrained robust and nonlinear control and set membership theory for control purposes, applied to vehicle stability control and the KiteGen project.

**Mario Milanese** ([mario.milanese@polito.it](mailto:mario.milanese@polito.it)) graduated in electronic engineering from the Politecnico di Torino, Torino, Italy, in 1967. Since 1980, he has been a full professor of system theory at Politecnico di Torino. From 1982 to 1987, he was head of the Dipartimento di Automatica e Informatica at the Politecnico di Torino. His research interests include identification, prediction, and control of uncertain systems with applications to biomedical, automotive, aerospace, financial, environmental, and energy problems. He is the author of more than 200 papers in international journals and conference proceedings. 